Ultraviolet−Visible Absorption Cross Sections of Gaseous HOBr

Trevor Ingham, Dieter Bauer, Jochen Landgraf, and John N. Crowley*

Max-Planck-Institut für Chemie, Division of Atmospheric Chemistry, P.O. Box 3060, 55020 Mainz, Germany

Received: November 20, 1997; In Final Form: February 18, 1998

The UV−visible absorption cross sections for HOBr between 260 and 545 nm have been measured at 295 K in either 80 or 300 Torr of He bath gas. HOBr was generated in situ by laser photolytic production of OH radicals in the presence of Br_2, and its absorption of light was detected using both a gated diode array camera (220 nm windows) and a photomultiplier. Calibration was performed relative to Br_2 loss. The UV−visible spectrum of HOBr consists of three broad absorption bands between about 240 and 550 nm, with λ_{max} at 284 nm ($\sigma = (25.0 \pm 1.2) \times 10^{-20}$ cm^2), 351 nm ($\sigma = (12.4 \pm 0.6) \times 10^{-20}$ cm^2), and 457 nm ($\sigma = (2.3 \pm 0.2) \times 10^{-20}$ cm^2). The existence of the third, long-wavelength absorption band has been confirmed unambiguously in this work. *J*-value calculations show that absorption into the third band is responsible for up to 50% of the total photolysis rate at high zenith angles close to the surface and at least 25% at all other altitudes and zenith angles down to 40°. At this zenith angle the total *J* value ranges from 3.2×10^{-3} s^{-1} at 15 km to 2.2×10^{-3} s^{-1} at the surface, corresponding to lifetimes of 5.2 and 7.6 min, respectively.

1. Introduction

The presence of bromine in the atmosphere has an important impact on both tropospheric and stratospheric ozone concentrations. Reactive bromine radicals such as BrO take part[1] in synergistic reactions with the chlorine oxide radical (ClO) that contribute substantially[2] to the dramatic annual losses in polar stratospheric ozone known as the "ozone hole" and may contribute to the observed negative trend in mid-latitude ozone concentrations in the lower stratosphere.[3] Observations of very low ozone concentrations in boundary-layer air in the polar troposphere are also closely related to the presence of reactive bromine species.[4]

Organic bromine is introduced in the atmosphere partly as a result of industrial activity in the form of CH_3Br and the halons. These relatively unreactive species are transported into the stratosphere where they are photodissociated to release Br atoms, which are subsequently converted to BrO by reaction with O_3:

$$Br + O_3 \rightarrow BrO + O_2 \quad (1)$$

Major reactions[5] of BrO include its self-reaction and reaction with ClO or NO in radical propagation steps

$$BrO + BrO \rightarrow Br + \text{other products} \quad (2)$$

$$BrO + ClO \rightarrow Br + Cl + \text{other products} \quad (3)$$

$$BrO + NO \rightarrow Br + NO_2 \quad (4)$$

or reaction with NO_2 or HO_2 to form less reactive reservoir compounds.

$$BrO + NO_2 + M \rightarrow BrONO_2 + M \quad (5)$$

$$BrO + HO_2 \rightarrow HOBr + O_2 \quad (6)$$

The slow rate of reaction of Br atoms with CH_4 and non-methane hydrocarbons[6] and the photolytic instability of the reservoir species HOBr and $BrONO_2$ ensure that a large proportion of bromine in the stratosphere is in the form of the reactive species Br and BrO, and this explains why the small abundance of bromine compared with that of chlorine in the stratosphere (∼10−20 ppt bromine compared with ∼3 ppb chlorine[3]) is sufficient to contribute significantly to stratospheric ozone loss.

In combination with reactions 1 and 6 the photodissociation of HOBr is part of a catalytic, ozone-destroying cycle:

$$HOBr + h\nu \rightarrow OH + Br \quad (7)$$

$$OH + O_3 \rightarrow HO_2 + O_2 \quad (8)$$

As shown above, HOBr is formed during the day in the reaction between HO_2 and BrO radicals (reaction 6). A further mechanism for its formation involves the nighttime hydrolysis of $BrONO_2$, an important reservoir of inorganic bromine:[7]

$$BrONO_2\,(aq) + H_2O \rightarrow HOBr\,(aq) + HNO_3\,(aq) \quad (9)$$

The efficient conversion of $BrONO_2$ to HOBr at night[8] results in a rapid formation of OH[9] and Br at dawn due to reaction 7, resulting in a net conversion of H_2O to HOx.[7]

In the troposphere, bromine can be released by heterogeneous/liquid-phase reactions that convert bromide originating from sea salt into photolabile forms of inorganic bromine such as Br_2. Following its uptake onto particulate surfaces, HOBr is thought to play an important role in catalytic cycles[10,11] involving Br^- or Cl^-, e.g.,

$$HOBr\,(aq) + Cl^- + H^+ \rightarrow BrCl\,(aq) + H_2O \quad (10)$$

$$BrCl\,(aq) + Br^- \rightarrow Br_2\,(aq) + Cl^- \quad (11)$$

Owing to its low solubility Br_2 (aq) is released into the gas phase where it is rapidly photolyzed:

$$Br_2 + h\nu\,(+2O_3) \rightarrow 2BrO + 2O_2 \quad (12)$$

$$BrO + HO_2 \rightarrow HOBr + O_2 \quad (6)$$

S1089-5639(98)00272-2 CCC: $15.00
Published on Web 04/22/1998

Clearly, the photolysis of HOBr, reaction 7, plays an important and direct role in ozone depletion in the stratosphere and indirectly influences the rate of heterogeneous processing of bromide and thus the amount of reactive bromine in the troposphere. The rate of photodissociation of HOBr is thus an important parameter in photochemical models that attempt to simulate the chemistry of the lower stratosphere or the marine boundary layer. Previous measurements of the UV−visible cross sections of HOBr are in poor agreement (see later), and the aim of the present work was to measure the absorption spectrum of HOBr using a novel approach that bypasses the difficulties associated with handling and purification of this compound.

2. Experimental Section

The pulsed laser photolysis/UV−visible absorption apparatus used throughout this work has been described elsewhere,[12] and only the details pertinent to the present study are given here. A 1.3 m long cylindrical Pyrex cell of 5 cm internal diameter equipped with quartz end windows was used as reaction vessel and optical absorption cell. Dielectric mirrors enabled the photolysis beam (KrF excimer laser, 248 nm, 20 ns pulse width) and the analysis light (D_2 and halogen lamps) to be overlapped collinearly along the cell's major axis. A further dieletric mirror situated behind the exit window reflected the photolysis beam back through the cell, thereby doubling the absorption path length and yield of OH.

To minimize diffusion, the analysis light sampled only a small central section of the volume swept out by the laser beam. The intensity of the unattenuated analysis light (I_0) was recorded over a 5 ms period just prior to the laser pulse. The postphotolysis analysis light intensity (I) was recorded using a diode array with 704 active pixels, which was gated from 0.06 to 5.06 ms after the laser pulse. The initial delay of 0.06 ms ensured that no fluorescence from the filters or glass surfaces (caused by the laser) was detected. The postphotolysis absorption was calculated from absorption $= \ln(I_0/I)$. Since I_0 and I were measured very close in time, the spectrum is not affected by long-term drifts in analysis light intensity or small fluctuations in gas concentrations.

Two spectral windows (with 80 nm overlap) covered the wavelength range 260−600 nm, and the wavelength axis was calibrated to an accuracy of 0.3 nm using the emission lines of a Hg pen-ray lamp. The final measurements consisted of the coaddition of 5000 laser pulses from five separate experiments. Also, time-resolved photomultiplier (PMT) measurements were performed at several wavelengths and consisted of the coaddition of 100 laser pulses. Initial absorptions were obtained from the prompt PMT signal. The wavelength resolution for diode array and PMT measurements was approximately 1.2 and 2 nm, respectively.

HOBr was produced in situ by generating OH radicals in the presence of Br_2 by the 248 nm pulsed photolysis of H_2O_2 in a flowing system (reactions 13 and 14). At this wavelength the quantum yield[13] for OH production via reaction 13 is 2. The absorption cross sections of H_2O_2 and Br_2 at 248 nm are 8.9×10^{-20} and 5.9×10^{-21} cm^2, respectively,[5,14] and within our noise levels for a typical experiment, no photolysis of Br_2 is detected. Consistent with this, and based on the cross sections above, we estimate an upper limit of 1.5% for the loss of Br_2 by photolysis compared with that for reaction with OH (reaction 14) in the final measurements.

$$H_2O_2 + h\nu\ (248\ \text{nm}) \rightarrow 2OH \qquad (13)$$

$$OH + Br_2 \rightarrow HOBr + Br \qquad (14)$$

Reactant concentrations in the range $[H_2O_2] = (5-20) \times 10^{15}$ cm^{-3} and $[Br_2] = (5-10) \times 10^{15}$ cm^{-3} were employed, and it was possible to generate around $(1-4) \times 10^{14}$ cm^{-3} OH radicals in a single laser pulse (approximate fluences between 20 and 60 mJ cm^{-2}), as calculated from the loss of Br_2 due to reaction 14. The room-temperature rate constants[5] $k_{14} = 4.2 \times 10^{-11}$ cm^3 s^{-1} and $k_{15} = 1.7 \times 10^{-12}$ cm^3 s^{-1} ensured that over 97% of OH radicals were converted into HOBr in less than 6 μs via reaction 14, with less than 3% contribution from reaction 15.

$$OH + H_2O_2 \rightarrow HO_2 + H_2O \qquad (15)$$

This was confirmed by time-resolved PMT measurements, which show that there is prompt loss of Br_2 and prompt formation of HOBr following the laser pulse.

In initial experiments where [OH] was high and $[Br_2]$ was low (see above), reaction 16 accounted for a fractional OH loss of around 0.002. The O atoms generated in reaction 16 lead to additional Br_2 loss and, more significantly, to BrO radical formation via reaction 17. The rate constants[5,15] for reactions 16 and 17 are 1.9×10^{-12} and 2.0×10^{-11} cm^3 s^{-1}, respectively, at 295 K. Under these conditions, the structured BrO absorption ($[BrO] < 3 \times 10^{11}$ cm^{-3}) was clearly observed superimposed on the HOBr absorption near 350 nm. At these low concentrations of BrO, there is no significant self-reaction over the period of the diode array gate (<1%).

$$OH + OH \rightarrow O + H_2O \qquad (16)$$

$$O + Br_2 \rightarrow BrO + Br \qquad (17)$$

For final measurements, (high $[H_2O_2]$ and high $[Br_2]$) the absorption due to BrO was barely discernible and contributed only 1−2% of the total absorption near 350 nm. To deconvolute this very small absorption due to BrO from that of HOBr, a reference BrO spectrum was recorded with the diode array at the same instrument resolution. BrO was generated by the 248 nm photolysis of O_3 in the presence of N_2 and Br_2 (reaction 17). Since only the shape of the BrO absorption was required for stripping purposes, no attempt was made to calibrate the spectrum. We note, however, that the relative spectrum was in reasonable agreement with literature,[5] considering the different resolutions used.

H_2O_2 was introduced into the cell by passing a flow of He through a thermostated bubbler containing liquid H_2O_2. A flow of Br_2 was generated by passing He over the surface of liquid Br_2 maintained at ambient temperature in a second bubbler. All gas flows were regulated by mass flow meters, and the concentration of the reactants was determined by absorption measurements at 220 nm for H_2O_2 ($\sigma = 2.19 \times 10^{-19}$ cm^2)[5] and at 416 nm for Br_2 ($\sigma = 6.52 \times 10^{-19}$ cm^2).[14] With total pressures between 80 and 300 Torr and flow rates between 3 and 12 L (STD) min^{-1} (slm), the residence time in the cell was about 5 s. The time between the laser pulses was usually about a factor of 2 greater than the residence time, thus ensuring that the photolysis products were removed prior to the next pulse. The stated purities of Br_2, He, and N_2 were 99.5% (Aldrich), 99.996% (Linde), and 99.996% (Linde), respectively. The H_2O_2 (80 wt %) was supplied by Solvay Interox and was concentrated to >90 wt % by passing He through the liquid for several days prior to use. All experiments were performed at 295 ± 2 K.

3. Results

To obtain the absorption due to HOBr, the postphotolysis absorption (see Figure 1) had to be corrected for the loss of both Br_2 and H_2O_2 and also for the formation of the BrO radical.

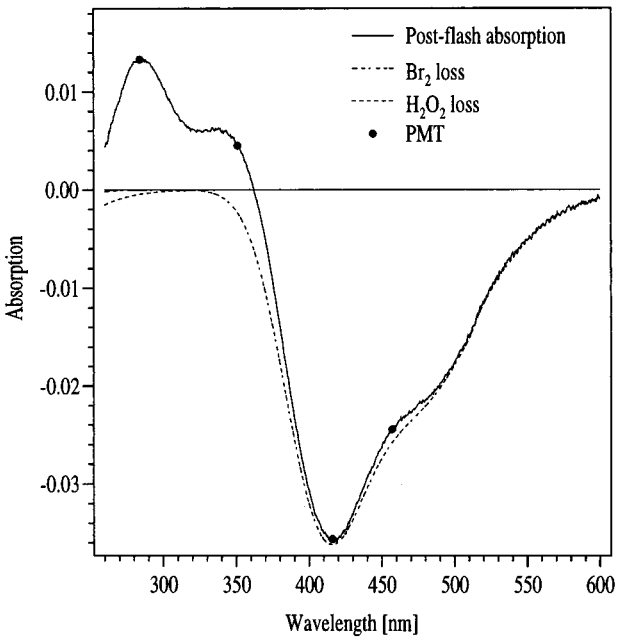

Figure 1. Postflash absorption (solid line) recorded with the diode array and prompt absorption obtained from time-resolved PMT measurements at several wavelengths (circles). Also shown is absorption due to Br_2 loss (broken line) and the calculated absorption due to H_2O_2 loss (dotted line). A total of 5000 laser shots (fluence of ~50 mJ cm^{-2}) in five separate experiments at 80 Torr were coadded to improve signal to noise. $[H_2O_2]_0$ was *2.0* $\times$ 10^{16} cm^{-3}. $[Br_2]_0$ was 1.0 $\times$ 10^{16} cm^{-3}.

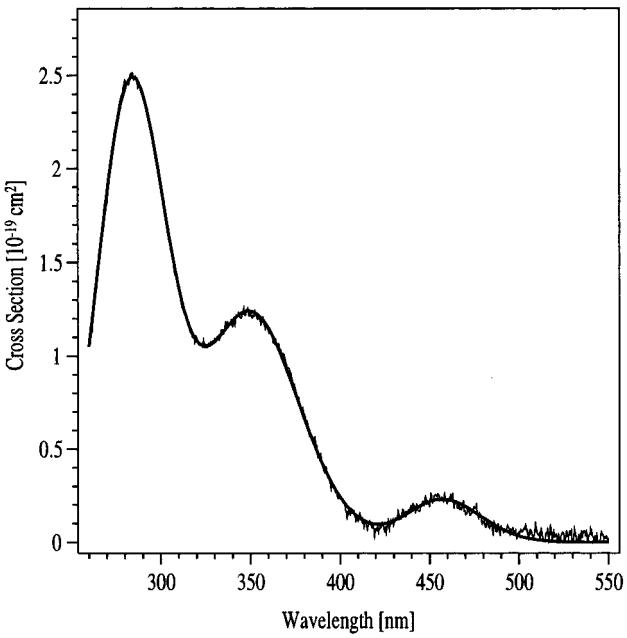

Figure 2. UV−visible cross sections obtained from this work together with the three-band Gaussian fit. The fit parameters are given in Table 1.

The reference spectrum used to correct for negative absorption due to Br_2 loss (ΔBr_2) was measured in the same experimental system (under the same conditions as those of the photolysis measurements) at the same instrument resolution and normalized to the cross sections of Maric et al.[14] ΔBr_2 absorption was corrected by fitting the reference spectrum to the postphotolysis absorption in the wavelength region 560−600 nm where HOBr has been shown[16] not to absorb. A small correction (~5% at 284 nm) for the loss of H_2O_2 in the short-wavelength region was performed by measuring the loss of Br_2 (see below) and equating this to the initial [OH], which is 200% of the H_2O_2 lost in the flash. Account was also taken of the slight H_2O_2 loss via reaction 15. The negative absorption due to H_2O_2 loss was then calculated using literature[5] cross sections. Following these corrections, the resulting HOBr (and small BrO) absorption was fitted with a function that included a Gaussian fit for each band and a scaling factor for the BrO reference spectrum. The scaling factor that resulted in the best fit (i.e., the removal of the pronounced vibronic structure due to BrO) was then used to subtract the BrO absorption.

Once corrected for the presence of Br_2, H_2O_2, and BrO, the absorption due to HOBr only was converted to a cross section by equating the loss of Br_2 (calculated from absorption changes at 550 nm $< \lambda <$ 600 nm where HOBr does not absorb) to the formation of HOBr as shown by reaction 14 (the loss of Br_2 via reaction 17 is negligible; see later).

Figure 1 shows the excellent agreement between the post-photolysis absorption measured with the diode array (solid line, average of 5000 laser pulses) and the prompt signals obtained from the time-resolved PMT measurements (solid circles). Also shown are the fitted Br_2 reference spectrum (broken line) used for cross section calibration and the calculated loss of H_2O_2 (dashed line), which were subsequently subtracted. On this scale it is not possible to see the absorption due to BrO.

A number of diagnostic tests were carried out, which included variation of reactant concentration and laser energy, in order to test for potential systematic errors in either the generation of HOBr or the spectral deconvolution procedure outlined above. All variations in reactant concentration (see above) and laser energy (factor of 3) were not found to influence the form of the HOBr spectrum. The only small change observed was in the relative amount of BrO radical production. However, when this was subtracted, the form and cross sections of the HOBr spectrum were highly reproducible.

Figure 2 shows the HOBr cross sections obtained from this work together with a Gaussian fit for each absorption band. As shown, the UV−visible spectrum of HOBr consists of three broad absorption bands between about 240 and 550 nm, with λ_{max} at 284 nm ($\sigma = (25.0 \pm 1.2) \times 10^{-20}$ cm^2), 351 nm ($\sigma = (12.4 \pm 0.6) \times 10^{-20}$ cm^2), and 457 nm ($\sigma = (2.3 \pm 0.2) \times 10^{-20}$ cm^2). The errors are derived from a consideration of potential systematic errors resulting from the method of HOBr calibration relative to Br_2 loss, and include uncertainty in the Br_2 cross sections (less than ±4%), and the errors introduced via Br-atom recombination and Br_2 photolysis, which are estimated as <1% and <1.5%, respectively. No error is introduced from small variations of reactant concentration and laser energy during the measurements. Furthermore, the errors that result from diffusion and the procedure used to strip the small BrO absorption are negligible.

The form of the Gaussian fit for each band is given by

$$\sigma(\lambda) = \sigma_{max} \exp\left\{-\mathrm{FW}\left[\ln \frac{\lambda_{max}}{\lambda}\right]^2\right\} \qquad \text{(I)}$$

where $\sigma(\lambda)$ is the cross section at wavelength λ, σ_{max} and λ_{max} are the cross section and wavelength at maximum absorption, and FW is a width parameter. The best-fit parameters for the cross sections determined in this work are shown in Table 1, which allow the calculation of the cross section at any wavelength. Table 2 shows the cross sections in 5 nm intervals. Since the vibrational frequency of the O−Br stretch (which should approximate the photoexcitation coordinate of HOBr) is high (~623 cm^{-1})[17,18] and since the thermal population of vibrational states other than $v = 0$ is expected to be very small,

TABLE 1: Gaussian Fit Parameters of the Cross Sections Determined in This Work[a]

	$10^{20}\sigma_{max}$, cm^2	λ_{max}, nm	FW
first band	24.8	284	109.8
second band	12.2	351	93.6
third band	2.28	457	242.4

[a] $\sigma(\lambda)$ is the cross section at wavelength λ. σ_{max} and λ_{max} are the cross section and wavelength at maximum absorption, respectively, and FW is a width parameter. The absorption spectrum between 240 and 550 nm is described by $\sigma(\lambda) = \sigma_{max}^{1st} \exp\{-FW^{1st}[\ln(\lambda_{max}^{1st}/\lambda)]^2\} + \sigma_{max}^{2nd} \exp\{-FW^{2nd}[\ln(\lambda_{max}^{2nd}/\lambda)]^2\} + \sigma_{max}^{3rd} \exp\{-FW^{3rd}[\ln(\lambda_{max}^{3rd}/\lambda)]^2\}$.

TABLE 2: HOBr Cross Sections Determined in This Work[a]

λ, nm	$10^{20}\sigma$, cm^2	λ, nm	$10^{20}\sigma$, cm^2	λ, nm	$10^{20}\sigma$, cm^2
260	10.5	360	11.5	460	2.28
265	14.6	365	10.5	465	2.14
270	18.7	370	9.32	470	1.91
275	22.1	375	8.00	475	1.62
280	24.3	380	6.66	480	1.30
285	25.0	385	5.38	485	0.993
290	24.0	390	4.22	490	0.723
295	21.9	395	3.24	495	0.502
300	19.1	400	2.43	500	0.334
305	16.2	405	1.80	505	0.212
310	13.6	410	1.36	510	0.129
315	11.8	415	1.08	515	0.075
320	10.8	420	0.967	520	0.0422
325	10.5	425	1.00	525	0.0228
330	10.8	430	1.15	530	0.0118
335	11.3	435	1.40	535	0.0059
340	11.9	440	1.68	540	0.0029
345	12.3	445	1.96	545	0.0001
350	12.4	450	2.18		
355	12.2	455	2.28		

[a] Calculated from the fit parameters given in Table 1.

the temperature dependence of the cross sections between 200 and 300 K is expected to be negligible.

4. Discussion

The calibration of the HOBr cross sections was performed by measuring the postflash Br_2 loss and equating this to HOBr formation, and it is necessary to consider any process that may falsify this method. One potential source of error is the recombination of Br atoms to re-form Br_2 on the time scale of the diode array measurements.

$$Br + Br + M \rightarrow Br_2 + M \qquad (18)$$

A room temperature, effective bimolecular rate constant of $k_{18} = 8.3 \times 10^{-15}$ cm^3 s^{-1} is obtained at 80 Torr (the pressure at which most experiments were conducted) from the expression given by Baulch et al.[19] for M = He. For the range of concentrations employed at 80 Torr, it can be shown that a maximum error of just 1% in the measurement of Br_2 loss can occur on the diode array time scale. This was confirmed in time-resolved PMT measurements by monitoring the Br_2 concentration at 416 nm. Additional PMT measurements were carried out for the same flowing mixture at 284, 351, 416, and 457 nm by scanning the monochromator between laser pulses (these wavelengths cover the first, second, and third λ_{max} of HOBr and λ_{max} of Br_2). Thus, any slight variation in reactant concentration or laser energy will not affect this measurement. Although HOBr absorbs very slightly at 416 nm (λ_{max} of Br_2), this results in an error of less than 1% in the measured $\Delta[Br_2]$ at this wavelength. There is excellent agreement between the prompt signals from these PMT measurements and diode array measurements taken between 0.06 and 5.06 ms after the flash (see Figure 1). In addition, after correction for enhanced Br-atom recombination, experiments carried out at 300 Torr yielded identical results, indicating that diffusion of HOBr was unimportant.

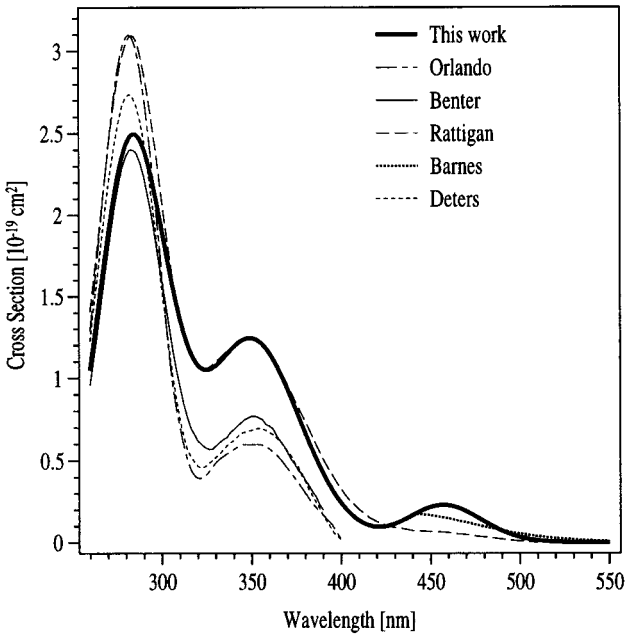

Figure 3. Absorption cross sections from the present study (bold solid line) and previous data from Orlando and Burkholder,[21] Benter et al.,[22] Rattigan et al.,[23] Deters et al.,[24] and Barnes et al.[16] The relative spectrum from Barnes et al.[16] has been normalized to the present cross section at 355 nm.

An assumption inherent to the present method of calibration is that each Br_2 loss produces one HOBr. The exclusive formation of HOBr and Br atoms via reaction 14 was determined by Loewenstein and Anderson.[20] Since the fractional loss of OH via reaction 16 is less than 0.002 of that via reaction 14, the subsequent fractional Br_2 loss via reaction with the resultant $O(^3P)$ atoms (reaction 17) is less than 0.001 of the Br_2 loss via reaction 14. As already stated, <1.5% of Br_2 loss is due to photolysis at 248 nm when compared with loss via reaction with OH.

Previous measurements[21−24] of the UV−visible absorption cross sections of HOBr are shown in Figure 3, along with the fit to the data of Figure 2 from the present study. The previous investigations have used either static equilibrium mixtures of $Br_2O/H_2O/HOBr$,[21,23,24]

$$Br_2O + H_2O \leftrightarrow 2HOBr \qquad (19, -19)$$

or wet synthetic generation and elution from aqueous solution into a slow-flowing system.[22] Both of these methods require that the measured optical density is corrected for the strongly absorbing and omnipresent Br_2O impurity. Since the cross sections of Br_2O at ca. 350 nm are an order of magnitude greater than those of HOBr at this wavelength, even small impurities require considerable correction. At equilibrium, some 80% of absorption at 350 nm is due to Br_2O,[23] and the shape of the HOBr spectrum will depend strongly on the amount of Br_2O subtracted from the optical density measurements of the equilibrium mixture. As discussed by Rattigan et al.,[23] the use of different methodologies for the stripping procedure, and Br_2O spectra of varying shape and intensity, is the main reason for the different shapes of HOBr absorption obtained in these experiments.

The conversion of optical density (corrected for Br_2O) to an absorption cross section for HOBr has been carried out relative to the loss of Br_2O upon addition of H_2O to a gas-phase Br_2O sample.[21,23,24] This method requires accurate Br_2O cross sections. The reported HOBr cross sections at the first maximum at ca. 280 nm (which should be free from absorption by Br_2O) vary from $\sim 2.4 \times 10^{-19}$ to 3.1×10^{-19} cm^2. As stated by Orlando and Burkholder,[21] the derived cross sections of HOBr scale linearly with that of Br_2O. Indeed, considering the $\sim$10−20% difference in the measured Br_2O cross sections by Orlando and Burkholder[21] and Rattigan et al.[23] at $\lambda < 400$ nm, the apparent good agreement between their HOBr spectra at 280 nm is misleading. Using the cross sections of Br_2O of Rattigan et al.[23] would decrease the Orlando and Burkholder[21] cross sections at 280 nm from 3.1×10^{-19} cm^2 to between 2.8×10^{-19} and 2.5×10^{-19} cm^2, in line with the present results and also those of Deters et al.[24] and Benter et al.[22]

Benter et al.[22] used an alternative approach and determined HOBr concentrations using gas-phase (HOBr + Cl) or aqueous phase (iodometric) titration schemes. Although indirect, both methods are independent of Br_2O cross sections and deliver consistent results of $\sigma_{283\ nm} = (2.4 \pm 0.1) \times 10^{-19}$ cm^2 (gas phase) and $(2.6 \pm 0.5) \times 10^{-19}$ cm^2 (iodometric).

There exists not only uncertainty in the value of σ at $\sim$280 nm, but the scatter about the second maximum is more substantial, with the measured values ranging from $\sim 0.6 \times 10^{-19}$ to 1.2×10^{-19} cm^2. Once again, this problem is associated with the presence of strongly absorbing Br_2O, which has maxima in its absorption bands between 315 and 350 nm. Also, assumptions used in stripping impurities such as Br_2O and Br_2 and use of restricted wavelength ranges have precluded the detection of the third band of HOBr in the above studies.

Barnes et al.[16] overcame the problems outlined above by measuring the relative amounts of OH generated in the photolysis of flowing $Br_2/Br_2O/HOBr/H_2O$ mixtures as a function of laser wavelength between 440 and 600 nm. Assuming a quantum yield of unity for OH formation at these wavelengths and at 355 nm, these authors derived an absorption spectrum (relative to 355 nm) free of interference from Br_2O (Br_2O cannot dissociate to give OH) and made the first detection of the third absorption band of HOBr beyond 400 nm. However, the quantum yield for Br ($^2P_{3/2}$) formation of >0.95 in HOBr photolysis at 363 nm (Benter et al.[22]) was calculated using an HOBr cross section of 0.67×10^{-19} cm^2 at this wavelength. Benter et al. suggest that formation of Br ($^2P_{1/2}$) is unimportant at 363 nm and conclude that the total Br formed is equal to that formed in the ground state, Br ($^2P_{3/2}$), and this can be equated to the amount of OH formed (assuming that HOBr dissociates to form only OH and Br). By use of our cross section at the same wavelength $\sigma_{HOBr}^{363nm} = 1.08 \times 10^{-19}$ cm^2, the quantum yield becomes >0.59. Clearly, the assumption of unity quantum yield for OH formation in HOBr photolysis has not been confirmed experimentally. It should, however, be noted that for OH formation in both HOI and HOCl photolysis, quantum yields close to unity have been obtained,[12,25−27] and by analogy, this is probably true also for HOBr.

There are a number of observations that give us confidence in the cross sections presented here. First, none of the problems outlined above for previous determinations occur in the present system. There is no contamination from Br_2O. By analogy with the $Cl_2O/H_2O/HOCl$ system,[28] the formation of Br_2O in reaction −19 is expected to take place mainly on the walls of the reaction vessel and not as a bimolecular gas-phase reaction in the short times after the laser flash during which our signal was aquired. In our experiments, total absorption is taken 0.06−5.06 ms after the laser pulse, which precludes the possibility that HOBr can diffuse to the wall and react to form Br_2O (which must diffuse back into the analysis light) on this time scale. Furthermore, the variation of laser energy (or H_2O_2 concentration) by over a factor of 3 should result in a 3-fold increase in the initial HOBr concentration and thus, according to reaction 19, to an increase in the rate of Br_2O formation of a factor of 9. Since no change in shape was observed in the region of maximum absorption by Br_2O, we conclude that its contribution to absorption is negligible. The form of the spectrum was also unaffected when the time between laser pulses was reduced to about $^1/_3$ of the cell residence time; thus, any buildup of Br_2O product was insignificant. Even under such deoptimized conditions, with noise levels in the single spectra (Figure 1) of $\sim 10^{-4}$ absorption units, we can place a conservative upper limit of 2×10^{12} Br_2O in 4×10^{14} HOBr, or 10% of the total absorption at 350 nm. For experiments using slow repetition rates and low energies, this can be reduced to <2%. Also, the time-resolved HOBr profiles at $\sim$351 and 284 nm showed the same time dependence to 20 ms. A significant formation of Br_2O on this time scale would have perturbed the 350 nm profile, but not that at 284 nm, and can thus be ruled out.

In addition, we find that the relative height of the second and third absorption bands agrees reasonably well with Barnes et al.,[16] whose spectrum, as described above, cannot be contaminated by Br_2O. However, owing to energy limitations around 440 nm, the $\lambda_{max} = 437$ nm of Barnes et al.[16] (calculated from the best-fit parameters given in ref 16) was obtained by extrapolation of a Gaussian profile through a noisy region of their relative spectrum and is blue-shifted by $\sim$20 nm when compared with results of the present study. This third band is thought to be due to excitation to a triplet state of HOBr, a view that is supported by a recent ab initio calculation[29] that indicates the existence of a dissociative triplet state in this wavelength region.

Since there is excellent agreement between the diode array measurements and the PMT measurements at the three HOBr absorption maxima, and our diagnostic test have shown that there is no measurable contamination by Br_2O, we conclude that the relative heights of the three absorption bands are defined accurately in our work.

***J*-Value Calculations**. To calculate the atmospheric photolysis rate constant (*J* value) for HOBr, the integral

$$J_{HOBr} = \int_{260nm}^{550nm} \sigma_{HOBr}(\lambda) F_{act}(\lambda)\, d\lambda \qquad \text{(II)}$$

was evaluated, which implicitly assumes a quantum yield of unity throughout the stated wavelength range. The actinic flux $F_{act}(\lambda)$ is calculated with the radiative transfer model DISORT,[30] and for large solar zenith angles the spherical geometry of the atmosphere is taken into account by employing the air mass factor correction of Kasten and Young.[31] A more detailed description of the *J*-value calculations can be found in Landgraf and Crutzen.[32]

Calculations were performed to evaluate the contribution of the third absorption band of HOBr, centered at 457 nm, to the overall dissociation rate constant. This was carried out by using either the full spectrum measured in this work or one truncated at 417.5 nm. As expected, the greatest contribution of the long-wavelength absorption band occurs at large zenith angles (e.g., at sunrise) where it accounts for almost 50% of absorption of the actinic flux. This contribution sinks to $\sim$25% in regions of

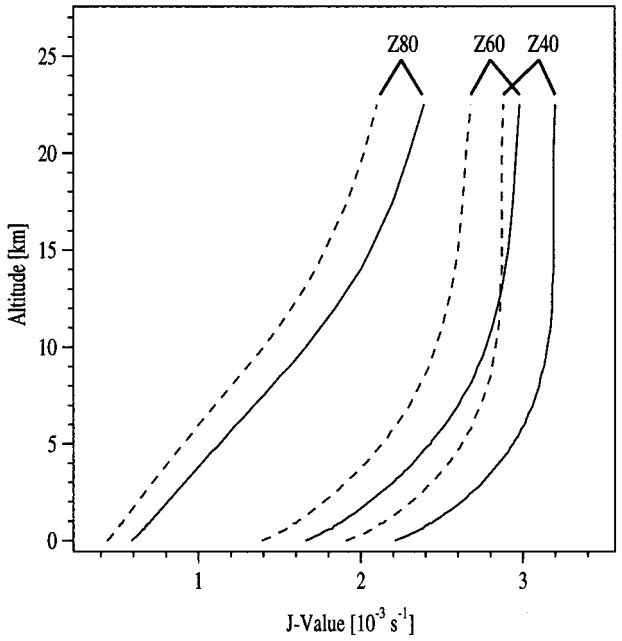

Figure 4. *J* values for HOBr calculated using the present data (solid lines) and also with the most recent recommendation[5] (dotted lines), which is based on the work of Rattigan et al.[23] (see text for details). An O_3 column of 300 dobson units was used. Z40, Z60, and Z80 refer to solar zenith angles of 40, 60, and 80°, respectively.

the atmosphere where more highly energetic radiation is available to dissociate HOBr in its stronger absorption band at 351 nm.

Figure 4 shows the *J* values of HOBr calculated using the cross sections determined in this work and those calculated using the presently recommended spectrum of Rattigan et al.[23] The new cross sections result in a decrease in the lifetime of HOBr in all parts of the atmosphere, which now ranges from 5 min at 15 km and 40° zenith angle to ~30 min at the earth's surface at 80° zenith angles. This short lifetime of HOBr has a number of implications for the ozone chemistry of both the lower stratosphere and the marine boundary layer. Under the assumption of efficient heterogeneous conversion of $BrONO_2$ to HOBr on sulfate aerosol in the lower stratosphere, HOBr comprises ~100% of total inorganic bromine at night and ~30% at noon.[8] A high photolysis rate for HOBr will convert a greater proportion of HOBr to the reactive Br and BrO radicals, which is expected to lead directly to more rapid O_3 loss rates. In addition, the simultaneous enhancement in OH will lead to faster rates of conversion of HCl to Cl atoms, and thus to a further, indirect contribution to O_3 depletion. For the marine boundary layer, the effect on O_3 is expected to be in the opposite direction. As discussed in the Introduction, the oxidation of bromide via heterogeneous HOBr reactions on, for example, sea-salt aerosol can play an important role in maintaining high concentrations of reactive bromine radicals in the remote marine boundary layer.[11] Since the photolysis of HOBr competes directly with its uptake into and reactions in aerosols, the considerably shorter photolysis lifetime calculated in this work (Vogt at al[11] used a 12 h daytime mean value of $J_{HOBr} = 3.5 \times 10^{-4}$ s^{-1}, based on the spectrum of Orlando and Burkholder[21]) will, under certain circumstances, result in a less efficient catalytic cycling of bromine and therefore lower levels of BrO and Br and reduced O_3 destruction rates. Detailed modeling studies of the atmospheric chemistry of HOBr, including the effects of the new *J* values reported here, are presently being conducted at this institute.

5. Conclusions

The UV−visible absorption cross sections of HOBr have been determined using an in situ gas-phase generation scheme that circumvents the problems associated with the presence of the strongly absorbing Br_2O impurity, which were encountered in previous studies. The calibration of the absorption cross sections was made relative to the well-known cross sections of Br_2. In addition to the known absorption bands at ~285 and 350 nm, we have directly detected absorption due to a third, weaker band centered at 457 nm. *J*-value calculations using the new absorption cross sections indicate that the lifetime of HOBr is reduced to ~5 min in the lower stratosphere (at zenith angle of 40 °) and to ~30 min at the surface at high zenith angles. These calculations assume quantum yield for dissociation of unity throughout the absorption spectrum, and experimental data to support this assumption are clearly required.

References and Notes

(1) McElroy, M. B.; Salawich, R. J.; Wofsy, S. C.; Logan, J. A. *Nature* **1986**, *321*, 759.
(2) Danilin, M. Y.; Sze, N. D.; Ko, M. W.; Rodriguez, J.; Prather, M. J. *Geophys. Res. Lett.* **1996**, *23*, 153.
(3) WMO/UNEP, 1994, World Meteorological Organisation-Global Ozone Research and Monitoring Project, Report No. 37; Geneva, 1995.
(4) Hausmann, M.; Platt, U. *J. Geophys. Res.* **1994**, *99*, 25399.
(5) DeMore, W. B.; Sander, S. P.; Golden, D. M.; Hampson, R. F.; Kurylo, M. J.; Howard, C. J.; Ravishankara, A. R.; Kolb, C. E.; Molina, M. J. JPL Publication 97-4; Jet Propulsion Laboratory: Pasadena, CA, 1997.
(6) Russell, J. J.; Seetula, J. A.; Gutman, D. *J. Am. Chem. Soc.* **1988**, *110*, 3092.
(7) Tie, X.; Brasseur, G. *Geophys. Res. Lett.* **1996**, *23*, 2505.
(8) Lary, D. J.; Chipperfield, M. P.; Toumi, R.; Lenton, T. *J. Geophys. Res.* **1996**, *101*, 1489.
(9) Salawich, R. J.; Wofsy, S. C.; Wennberg, P. O.; Cohen, R. C.; Anderson, J. G.; Fahey, D. W.; Gao, R. S.; Keim, E. R.; Woodbridge, E. L.; Stimpfle, R. M.; Koplow, P.; Kohn, D. W.; Webster, C. R.; May, R. D.; Pfister, L.; Gottlieb, E. W.; Michelsen, H. A.; Yue, G. K.; Prather, M. J.; Wilson, J. C.; Brock, C. A.; Jonsson, H. H.; Dye, J. E.; Baumgardner, D.; Proffitt, M. H.; Loewenstein, M.; Podolske, J. R.; Elkins, J. W.; Dutton, G. S.; Hintsa, E. J.; Dessler, A. E.; Weinstock, E. M.; Kelly, K. K.; Boering, K. A.; Daube, B. C.; Chan, K. R.; Bowen, S. W. *Geophys. Res. Lett*. **1994**, *23*, 2551.
(10) Fan, S. M.; Jacob, D. J. *Nature* **1992**, *359*, 522.
(11) Vogt, R.; Crutzen, P. J.; Sander, R. *Nature* **1996**, *383*, 327.
(12) Bauer, D.; Ingham, T.; Carl, S. A.; Moortgat, G. K.; Crowley, J. N. *J. Phys. Chem. A* **1998**, *102*, 2857.
(13) Vaghjiani, G. L.; Ravishankara, A. R. *J. Phys. Chem*. **1990**, *92*, 996.
(14) Maric, D.; Burrows, J. P.; Moortgat, G. K. *J. Photochem. Photobiol., A* **1994**, *83*, 179.
(15) Nicovich, J. M.; Wine, P. H. *Int. J. Chem. Kinet.* **1990**, *22*, 379.
(16) Barnes, R. J.; Lock, M.; Coleman, J.; Sinha, A. *J. Phys. Chem.* **1996**, *100*, 453.
(17) Schwager, I.; Arkell, A. J. *J. Am. Chem. Soc*. **1967**, *89*, 6006.
(18) McRae, G. A.; Cohen, E. A. *J. Mol. Spectrosc*. **1990**, *139*, 369.
(19) Baulch, D. L.; Duxbury, J.; Grant, S. J.; Montague, D. C. *J. Phys. Chem. Ref. Data* **1981**, *10* (Suppl. 1).
(20) Loewenstein, L. M.; Anderson, J. G. *J. Phys. Chem.* **1984**, *88*, 6277.
(21) Orlando, J. J.; Burkholder, J. B. *J. Phys. Chem.* **1995**, *99*, 1143.
(22) Benter, T.; Feldman, C.; Kirchner, U.; Schmidt, M.; Schmidt, S.; Schindler, R. N. *Ber. Bunsen-Ges. Phys. Chem.* **1995**, *99*, 1144.
(23) Rattigan, O. V.; Lary, D. J.; Jones, R. L.; Cox, R. A. *J. Geophys. Res.* **1996**, *101*, 23021.
(24) Deters, B.; Himmelmann, S.; Blindauer, C.; Burrows, J. P. *Ann. Geophys.* **1996**, *14*, 468.
(25) Molina, M. J.; Ishiwata, T.; Molina, L. T. *J. Phys. Chem*. **1980**, *84*, 821.
(26) Vogt, R.; Schindler, R. N. *J. Photochem. Photobiol., A* **1992**, *66*, 133.
(27) Butler, P. J. D.; Phillips, L. F. *J. Phys. Chem.* **1983**, *87*, 183.
(28) Knauth, H.-D.; Alberti, H.; Clausen, H. *J. Phys. Chem.* **1979**, *83*, 1604.
(29) Francisco, J. S.; Hand, M. R.; Williams, I. H. *J. Phys. Chem.* **1996**, *100*, 9250.
(30) Stamnes, K.; Tsay, S.-C.; Wiscombe, W.; Jayaweera, K. *Appl. Opt.* **1988**, *27*, 2502.
(31) Kasten, F.; Young, A. T. *Appl. Opt.* **1989**, *28*, 4735.
(32) Landgraf, J.; Crutzen, P. J. *J. Atmos. Sci*, in press.